

High-spin analog resonances near the $N = 50$ neutron shell

S. Galès, Y. El Hage, J. P. Schapira, S. Fortier, H. Laurent, and J. M. Maison

Institut de Physique Nucléaire, BP No. 1, 91406 Orsay, France

(Received 19 July 1979)

The $^{96}\text{Zr}(^3\text{He},d)^{97}\text{Nb}$ and the $^{92}\text{Mo}(^3\text{He},d)^{93}\text{Tc}$ reactions, investigated at, respectively, 39.0 and 28.5 MeV incident energies, were used to populate selectively high-spin analog resonances in ^{97}Nb and ^{93}Tc . Angular distributions were measured for the $d_{3/2}$, $g_{7/2}$, and $h_{11/2}$ analog states of the low-lying levels in ^{97}Zr . A distorted-wave Born-approximation analysis of the data for these unbound levels (using Gamow functions as form factors) was carried out and spectroscopic strengths extracted. The $^{96}\text{Zr}(^3\text{He},dp)$ and $^{92}\text{Mo}(^3\text{He},dp)$ reactions were performed, respectively, at 37.5 and 30 MeV incident energies. The angular distributions of the emitted protons were measured in coincidence using method II of Litherland and Ferguson with 0° detection of deuteron groups. Spins, population parameters, and proton branching ratios to the ground state and excited states of the targets were determined from the analysis of the angular correlation data. The position of the neutron threshold as compared with the excitation energies of the analog states in ^{97}Nb and ^{93}Tc is found to be an important parameter in the extraction of the structure information on core-excited components in the parent levels wave functions. Neutron particle-hole multiplets based on the $(d_{5/2})_n^{-1} \otimes (h_{11/2})_n^{+1}$ and $(d_{5/2})_n^{-1} \otimes (g_{7/2})_n^{+1}$ configurations are observed for the first time in ^{96}Zr through the decay of the $g_{7/2}$ and $h_{11/2}$ analog resonances. The limitation of the present method due to the neutron threshold or to the energy resolution in the proton channel is discussed and compared with the results of inelastic resonant scattering through isobaric analog resonances.

NUCLEAR REACTIONS $^{92}\text{Mo}(^3\text{He},d) E = 28.5$ MeV; measured $\sigma(E_d, \theta)$, $\theta = 20^\circ, 35^\circ$. $^{96}\text{Zr}(^3\text{He},d) E = 39.0$ MeV; measured $\sigma(E_d, \theta)$. $^{92}\text{Mo}(^3\text{He},d\bar{p}) E = 30$ MeV, $^{96}\text{Zr}(^3\text{He},d\bar{p}) E = 37.5$ MeV; measured $\sigma(E_d, E_p, \theta_p)$. ^{93}Tc , ^{97}Nb deduced IAS, L , J , π , S , Γ_p , $\Gamma_{p'}$. DWBA analysis using Gamow functions as form factors. Magnetic analysis. Enriched targets.

I. INTRODUCTION

As an extension of the experimental program on the population and the proton decay of isobaric analog states (IAS) in the f - p shell nuclei,^{1,2} through the study of the $(^3\text{He},d)$ and $(^3\text{He},d\bar{p})$ reactions, the present paper reports on the investigation of high-spin analog resonances near the $N = 50$ neutron shell. In that region of the mass table (Zr, Mo, etc.) high-spin IAS are not populated in proton elastic and inelastic resonant reactions and therefore could not be studied due to the low penetrabilities for large l values ($l=4, 5$) of the incident proton.

At a sufficiently high incident energy, high-spin analog resonances have been excited by means of proton stripping reactions on Zr and Mo targets³⁻⁶ with large cross sections (~ 1 mb/sr) at forward angles. Due to the matching conditions $l=0$ ($3s_{1/2}$), IAS are rather weakly populated, but these IAS have generally been studied in detail using the (p, p_0) , (p, p') , and $(p, p'\gamma)$ resonant channels.⁷⁻¹¹

In the case of the $^{92}\text{Mo}(^3\text{He},d)^{93}\text{Tc}$ reaction to unbound analog states, many papers have been published during the past few years^{4, 6, 12-15} on the distorted-wave Born approximation (DWBA) analysis of IAS using different methods for computing

the proton form factors. However, the investigation of the proton decay of the IAS using the $(^3\text{He},d\bar{p})$ process (here \bar{p} denotes the proton emission from the IAS) can be a powerful method to detect core-excited components in the parent state wave functions. Only one experiment has been reported on the proton decay of IAS in ^{93}Tc by means of the $^{92}\text{Mo}(^3\text{He},d\bar{p})^{92}\text{Mo}$ reaction,¹⁶ studied at a rather low incident energy ($E_i \sim 20$ MeV) and with poor energy resolution. No information has been obtained on the decay properties of the high-spin analog resonances ($g_{7/2}, h_{11/2}$). Moreover, the geometry adopted in the d - \bar{p} coincidence arrangement leads to a basic difficulty in the analysis of the angular correlation data.

As for the IAS in ^{97}Nb , a previous study of the $^{96}\text{Zr}(^3\text{He},d)^{97}\text{Nb}$ reaction at 30.2 MeV incident energy has been reported.⁵ The extracted spectroscopic factors using two different methods for computing the proton form factor were rather inconsistent with the (d, p) results.^{17, 18}

The present data were obtained with a split-pole spectrograph and analyzed using Gamow functions as form factors. This method has been shown to be quite successful in reproducing the single-particle strengths of IAS as compared to their parent levels in the f - p shell nuclei.^{1, 2}

No resonant reaction studies have been reported on the proton decay of IAS in ^{97}Nb . This decay is investigated for the first time using the $^{96}\text{Zr}(^3\text{He}, d\bar{p})$ reaction. Because of the large proton decay energy, deexcitations to the ground, collective, and neutron-particle hole states are expected. However, the IAS in ^{97}Nb are located well above the neutron threshold and therefore, low proton branching ratios could limit the accuracy of the measurements. In addition, the natural width of the IAS (30–50 keV) and the high counting rates in the proton detectors lead to typical energy resolutions of 100–150 keV in the proton coincident spectra. This value is too large compared, for example, to the neutron particle-hole multiplet spacing (~ 30 keV) and therefore only the total proton branching to these particular configurations could be measured in this kind of experiment.

II. EXPERIMENTAL PROCEDURE AND RESULTS

A. Spectrograph data

Self-supporting metal foils of ^{92}Mo and ^{96}Zr were bombarded, respectively, at 28.5 and 39 MeV incident energies by an ^3He beam delivered by the Orsay MP Tandem Accelerator. The targets were about $600 \mu\text{g}/\text{cm}^2$ thick and isotopically enriched to 99% ^{92}Mo and 72.5% ^{96}Zr (14.6% of ^{90}Zr). The outgoing deuterons were detected using four, solid state, $1000 \mu\text{m}$ thick, position sensitive detectors (PSD) in the focal plane of a split-pole spectrograph.

The data were recorded at 20° and 35° laboratory angles with the ^{92}Mo target. The magnetic field was set in order to obtain the ^{93}Mo ground-state analog in the first PSD, leading to the observation of the remaining IAS in the following detectors. The resulting spectra are displayed in Fig. 1. The excitation energies were obtained by a calibration of the radius ρ versus the channel number using a ThC α source. The results are

presented in Table I together with the one obtained in previous studies. The IAS are clearly observed as narrow peaks above a continuous background. In the vicinity of the IAS, one can notice the asymmetric shape of the background, especially for the $2d_{5/2}$ IAS at 8.41 MeV and the $1h_{11/2}$ IAS at 10.74 MeV. Such an effect is expected if there is a strong mixing between the “doorway” state and the surrounding high density of T_ζ “normal” states. In the case of IAS in ^{93}Tc , they are bound with respect to the neutron decay channel and only proton emission is energetically allowed for both T_ζ and T_ν levels. This situation is of importance if one wants to extract directly structure information on the parent levels. This point will be discussed in more detail in Sec. IV.

The $^{96}\text{Zr}(^3\text{He}, d)^{97}\text{Nb}$ reaction was studied at 39 MeV incident energy, using the same experimental setup discussed above. The deuteron spectrum in the excitation energy range where the IAS are expected is presented in Fig. 2. Three peaks at, respectively, $E_x = 14.43$, 14.65, and 15.64 MeV excitation energies in ^{97}Nb are clearly observed in that spectrum. On the basis of Coulomb displacement energies, they are assigned, respectively, as the analogs of the $J^\pi = \frac{3}{2}^+$, $E_x = 1.11$ MeV, $J^\pi = \frac{7}{2}^+$, $E_x = 1.27$ MeV, and $J^\pi = \frac{11}{2}^-$, $E_x = 2.26$ MeV levels in the ^{97}Zr parent nucleus.¹⁶ An attempt to observe the $3s_{1/2}$ ground-state analog has been made by moving the field in the spectrometer. The very bad angular momentum matching ($\Delta l = 4$) for that transition explains the nonobservation of the $3s_{1/2}$ ground-state analog. The energy resolution in the $^{96}\text{Zr}(^3\text{He}, d)^{97}\text{Nb}$ and the $^{92}\text{Mo}(^3\text{He}, d)^{93}\text{Tc}$ experiments was limited to 40 keV because of the target thickness and the natural width of the IAS.

Absolute cross sections were obtained by comparing the 39 MeV ^3He elastic scattering data at 10° and 12° laboratory angles with the cross section computed using the standard optical model to describe the entrance channel (see Sec. II). At these angles, the ratios of the calculated cross

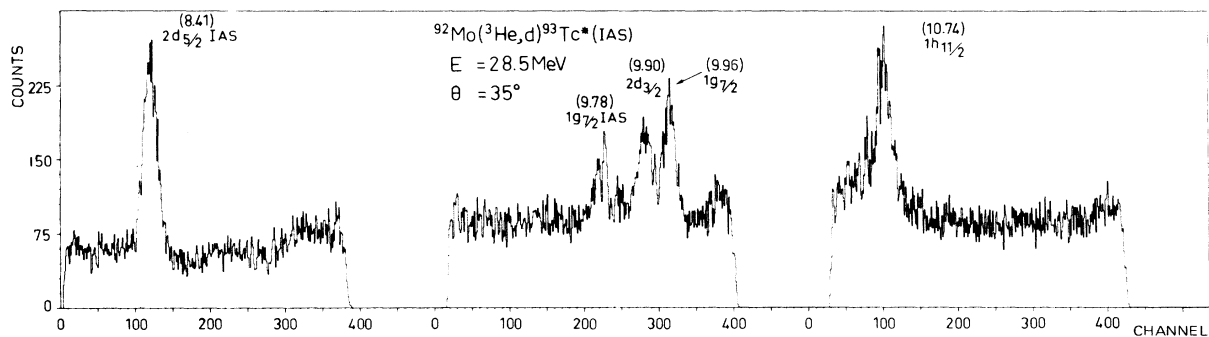


FIG. 1. Deuteron energy spectra from the $^{92}\text{Mo}(^3\text{He}, d)^{93}\text{Tc}$ reaction at 35° laboratory angle. The IAS in ^{93}Tc are clearly observed above a continuous background.

TABLE I. Summary of the results on IAS in ^{93}Tc populated through proton stripping or resonant reactions.

$E_x(\text{IAS})^a$ (MeV)	$E_p^{\text{c.m.}}^a$ (MeV)	l	J^π^b	Previous works ^b	$S(p, p_0)^c$	$S^>(^3\text{He}, d)^d$	$E_x(\text{Parent})^e$ (MeV)	$S_{d\beta}^e$
8.41	4.31	2	$\frac{5}{2}^+$	$(^3\text{He}, d), (d, n), (p, p_0)$	0.55	0.72, 0.87, 0.83	0.00	0.84
9.36	5.26	0	$\frac{1}{2}^+$	$(d, n), (p, p_0)$	0.60		0.95	0.64
9.78		4	$\frac{7}{2}^+$	$(^3\text{He}, d)$		0.28, 0.33, 0.32	1.36	0.26
9.90	5.80	2	$\frac{3}{2}^+$	$(^3\text{He}, d), (d, n), (p, p_0), (p, p')$	0.25	0.55, 0.43	1.50	0.50
9.96		4	$\frac{7}{2}^+$	$(^3\text{He}, d)$		0.15, 0.16	1.53	0.15
10.11	6.01	2	$\frac{5}{2}^+$	$(^3\text{He}, d), (p, p_0), (p, p')$		0.17	1.69	0.18
10.74		5	$\frac{11}{2}^-$	$(^3\text{He}, d)$		0.33, 0.47, 0.59	2.30	0.30

^a The excitation energies are from this work. The uncertainties are of ± 25 keV. The resonance energies in the center of mass of the $^{92}\text{Mo}+p$ system are deduced from the relation $E_p = E_x(\text{IAS}) - B_p$. Here B_p is the binding energy of the proton in ^{93}Tc taken equal to 4.10 MeV.

^b Angular momentum, spin, and parities of IAS in ^{93}Tc from previous works (Refs. 4 and 6–12).

^c Spectroscopic factors of IAS in ^{93}Tc deduced from the analyses of resonant reactions (Ref. 7).

^d DWBA analysis of unbound isobaric analog states in ^{93}Tc (Refs. 12, 14, and 15).

^e Excitation energies and spectroscopic strengths for the parent states from Ref. 17.

sections to Rutherford were found to be 1.04 and 1.02, respectively. These values are essentially invariant under relatively wide variations of the optical model parameters. The absolute cross sections are therefore estimated to be accurate to $\pm 10\%$.

B. Angular correlation data

The $^{92}\text{Mo}(^3\text{He}, d\bar{p})$ and the $^{96}\text{Zr}(^3\text{He}, d\bar{p})$ reactions have been performed, respectively, at 30 and

37.5 MeV incident energies using the same accelerator facilities described above. The targets were of the same nature as the ones used in the spectrograph experiments. The experimental arrangement used in the angular correlation experiments was essentially the same as the one described in detail in Ref. 1 and will be presented briefly in this paper.

The deuterons were detected near 0° with a triplet of magnetic quadrupole lenses.¹⁹ The entrance aperture of the 0° spectrometer subtends a solid

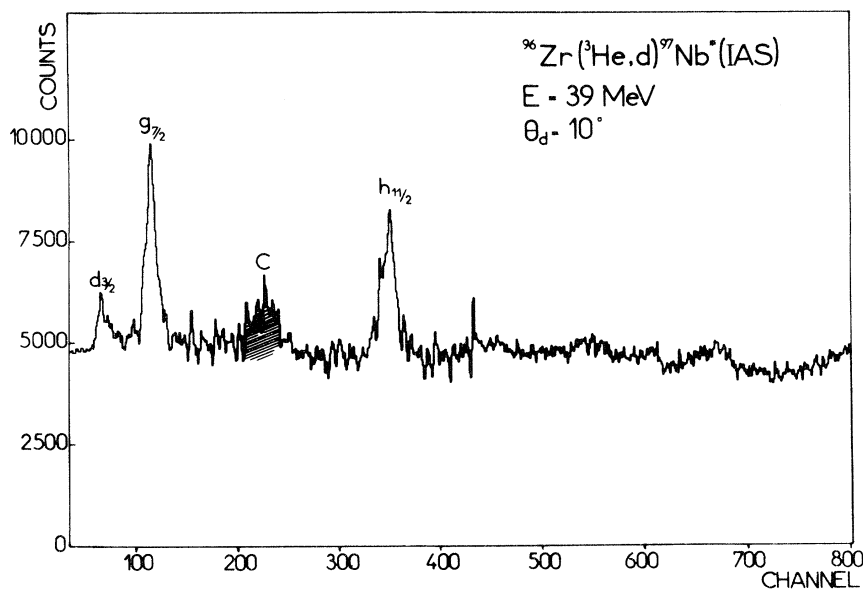


FIG. 2. Deuteron energy spectrum from the $^{96}\text{Zr}(^3\text{He}, d)^{97}\text{Nb}$ reaction at 10° laboratory angle. This spectrum consists of a juxtaposition of different PSD spectra taken at two different magnetic fields in the split-pole spectrograph.

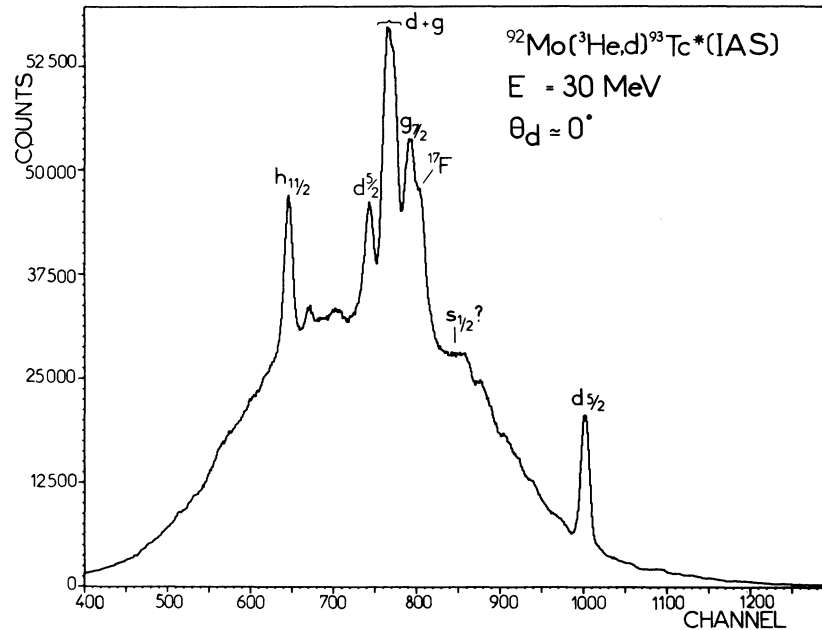


FIG. 3. Single deuteron spectrum from the $^{92}\text{Mo}(^3\text{He},d)^{93}\text{Tc}$ reaction taken near 0° with the triplet of magnetic quadrupole lenses.

angle of 12 msr at the maximum of the transmission curve. Reaction products were focussed onto a 300 mm^2 , $4000 \mu\text{m}$ thick Si(Li) detector cooled at -10°C . The single deuteron spectra observed near 0° are presented in Figs. 3 and 4. The energy resolution was about 50 keV full width at half maximum (FWHM).

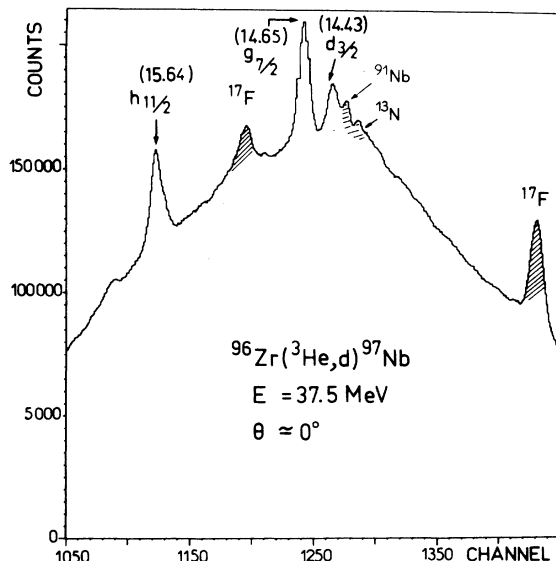


FIG. 4. Single deuteron spectrum for the $^{96}\text{Zr}(^3\text{He},d)^{97}\text{Nb}$ reaction. Some contaminant peaks from the $^{12}\text{C}(^3\text{He},d)$, $^{16}\text{O}(^3\text{He},d)$, and $^{90}\text{Zr}(^3\text{He},d)$ reactions are also observed.

The expected IAS in ^{93}Tc and ^{97}Nb are strongly excited and the resulting high cross sections for the population of these levels allow the investigation in coincidence of their particle decay. In both cases, the narrow peaks are superimposed on a high background with a typical bell shape reflecting the transmission curve of the 0° spectrometer. In the spectrum of Fig. 4, due to the large isotopic abundance of ^{90}Zr in the target, the $2d_{5/2}$ ground-state analog in ^{91}Nb is also observed. This level, bound with respect to the neutron channel, could only decay to the ground state of ^{90}Zr with a 100% branching ratio. This decay was used as a test in order to control the electronic losses due to the high counting rates in the proton detectors.

The coincident protons were detected in eight $1500 \mu\text{m}$ thick Si(Li) detectors cooled at -20°C and placed on a turnable plate in a scattering chamber. The solid angle of the proton detectors was of about 20 msr. Coincidence events were measured for proton laboratory angles ranging from 82° to 166° by increments of 10° to 15° . Each coincident event E_d, E_p, T_{d-p} (where E and T denote energy and time) was recorded on magnetic tape and processed off line on an IBM 360-75 computer.

Absolute normalization of the angular correlation data was obtained by accumulating simultaneously to the coincidence experiment a direct deuteron spectrum. After a time of flight correction, two dimensional spectra ($E_d - E_p$) were built up and random events subtracted. A typical two parameter spectrum is displayed in Fig. 5. We

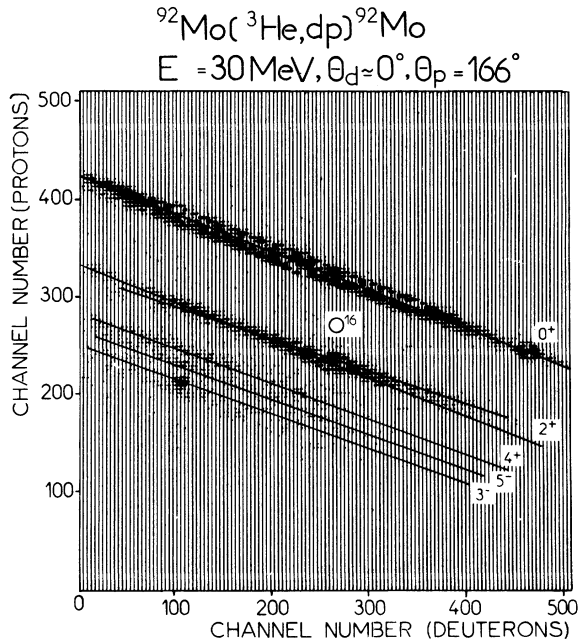


FIG. 5. Deuteron-proton coincidence spectrum in the $^{92}\text{Mo}(^3\text{He}, d\tilde{p})^{92}\text{Mo}$ reaction. The solid lines labeled 0^+ , 2^+ , 4^+ , 5^- , and 3^- refer to kinematic lines for the following reactions $^{92}\text{Mo}(^3\text{He}, d\tilde{p})^{92}\text{Mo}(\text{g.s.})$, $^{92}\text{Mo}(^3\text{He}, d\tilde{p})^{92}\text{Mo}(2_1^+)$, etc. Note that the kinematic line for the $^{16}\text{O}(^3\text{He}, d\tilde{p})^{16}\text{O}(\text{g.s.})$ process is mixed with the one of the $^{92}\text{Mo}(^3\text{He}, d\tilde{p})^{92}\text{Mo}(2^+)$ reaction.

clearly observe kinematic lines associated with the following processes: $^{92}\text{Mo}(^3\text{He}, d\tilde{p})^{92}\text{Mo}(0^+)$, $^{92}\text{Mo}(^3\text{He}, d\tilde{p})^{92}\text{Mo}(2^+)$ mixed with $^{16}\text{O}(^3\text{He}, d\tilde{p})^{16}\text{O}$ and other decays to higher excited states.

These kinematic lines were projected along the deuteron axis in order to produce ^{93}Tc levels decaying to the ground, first 2_1^+ , 4_1^+ , 5_1^- , and 3_1^- excited states of ^{92}Mo . The resulting spectrum is shown in Fig. 6. In this case, all the IAS in ^{93}Tc are bound with respect to the neutron decay channel. Therefore, the coincident deuteron spectrum displayed in Fig. 6 is very similar to the single spectrum of Fig. 3. One can notice the rather high background of $T_<$ states under the narrow peaks which characterize the $T_>$ levels. Therefore, the extraction of the proton branching ratios, especially to the ground and first 2^+ state, is expected to be strongly dependent on the proton decay of the "background" states.

A similar set of spectra could be built for the $^{96}\text{Zr}(^3\text{He}, d\tilde{p})^{96}\text{Zr}$ process. In Fig. 7, the kinematic lines to various final states in ^{96}Zr were projected separately along the deuteron axis. The different branchings of the $2d_{3/2}$, $1g_{7/2}$, and $1h_{11/2}$ IAS in ^{97}Nb appeared clearly on the figure. On the contrary, the IAS in ^{97}Nb are located well above the neutron threshold and therefore the surrounding

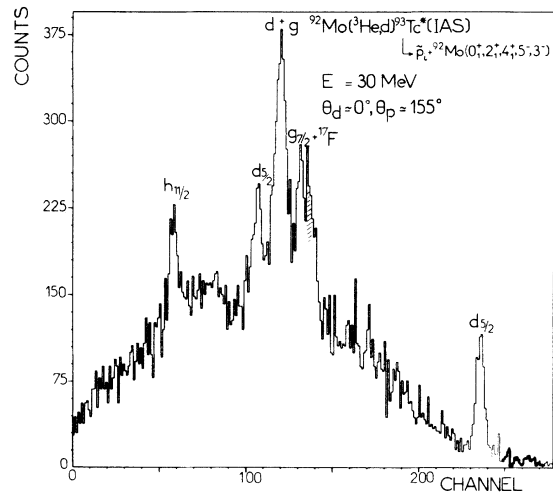


FIG. 6. Projection of kinematic lines $\tilde{p}(\text{g.s.})$, $\tilde{p}(2_1^+)$, etc., on the deuteron axis for the $^{92}\text{Mo}(^3\text{He}, d\tilde{p})^{92}\text{Mo}$ process. The IAS in ^{93}Tc decaying by proton emission are clearly observed.

background states preferentially decay via neutron emission. Only the IAS decays rather strongly via the isospin-allowed proton channel. This is reflected by the shape of the coincident deuteron spectra of Fig. 7 compared to the single spectrum displayed in Fig. 4. The $1h_{11/2}$ IAS shows a very weak proton branching to the ground state due to the large angular momentum of the emitted proton. The $2d_{3/2}$ and $1g_{7/2}$ IAS are observed to decay to the ground state (\tilde{p}_0) and to the first 2_1^+ excited state. Finally, two kinematic lines labeled $p_i + ^{96}\text{Zr}(p-h)$ in Fig. 7 show that the $1g_{7/2}$ and $1h_{11/2}$

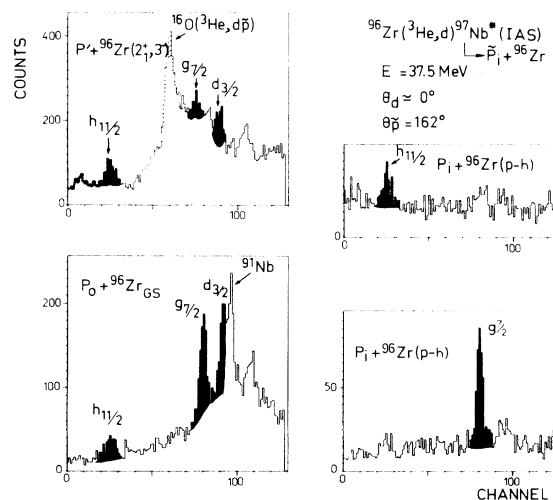


FIG. 7. Projection of kinematic lines $\tilde{p}(\text{g.s.})$, $\tilde{p}(2^+)$, etc., on the deuteron axis for the $^{96}\text{Zr}(^3\text{He}, d\tilde{p})^{96}\text{Zr}$ reaction. The proton decays to different final states of the ^{96}Zr nucleus are presented separately.

IAS have a significant branching to highly excited states of the target ($E_x \sim 4$ MeV). These final states will be proposed as neutron particle-hole configurations based on the ^{96}Zr ground state and will be discussed in detail in Sec. V.

III. DISTORTED WAVES ANALYSIS OF THE $^{96}\text{Zr}(^3\text{He}, d)^{97}\text{Nb}$ REACTION

A. General analysis

Angular distributions of transitions to three IAS in ^{97}Nb have been extracted from the experimental data. In order to carry out a DWBA analysis for these unbound levels, the proton form factor was calculated using complex energy eigenstates or Gamow functions $\tilde{g}_{l, \nu}(\tilde{r})$ following the method developed by Coker *et al.*¹⁴ and which leads to a single-particle cross section in a completely analogous way to the one derived for bound states. This method has been successfully applied to about 40 IAS in various f - p shell nuclei.^{1,2} The program GAMOW was used to compute the proton form factor. For a given lJ transition, the well depth of the proton potential was searched in order to obtain the complex energy $\tilde{E} = E_R - i\Gamma^{lJ}/2$ of the resonant state (E_R is the energy of the resonance in the center of mass system and Γ_{sp}^{lJ} is the single-particle width). It should be noticed here that the value of single-particle width Γ_{sp}^{lJ} is also directly obtained in the calculations.

Zero-range DWBA calculations with Gamow functions as form factors were performed using the computer code VENUS. Optical parameters used in the distorted wave calculations are listed in Table II. They are identical to the ones used by Finkel *et al.*⁵ in their analysis of the $(^3\text{He}, d)$ reaction to analog states in Nb isotopes.

B. Angular distributions and spectroscopic factors

The spectroscopic factors C^2S were extracted by comparing DWBA predictions with the measured

cross-section values

$$(\frac{d\sigma}{d\Omega})_{\text{expt}} = NC^2S\sigma_{\text{DW}}^{lJ}.$$

The usual normalization constant $N=4.42$ was used in the calculations. The results of the calculations are compared with the experimental angular distributions in Fig. 8. The shapes of experimental distributions are well reproduced by the DWBA calculations. The slopes obtained for different l transfers together with the maxima at forward angles (except for $l=5$) allow the identification of the transferred angular momentum. The extracted spectroscopic strengths C^2S are listed in Table III. They are compared with the one obtained by Finkel *et al.*⁵ and with the neutron single-particle strengths of their parent states.¹⁸ From deduced l values, spins, and parities, $(J)^\pi = (\frac{3}{2})^+$, $(\frac{7}{2})^+$, and $(\frac{1}{2})^-$ are proposed for the observed IAS on the basis of shell-model considerations. These results will be confirmed by the analysis of the angular correlation data (see Sec. IV). Assuming these spins and parities, the deduced spectroscopic factors $S^\gamma(^3\text{He}, d)$ listed in Table III are in good agreement with the ones obtained for the parent states except for the $1g_{7/2}$ analog pair where the discrepancy between $S^\gamma(^3\text{He}, d)$ and $S_{d,p}$ reaches 50%. However, results of this analysis of the $^{96}\text{Zr}(^3\text{He}, d)^{97}\text{Nb}$ reaction lead to spectroscopic strengths for the IAS in a closer agreement with the neutron single-particle strengths than the values obtained previously by Finkel *et al.*⁵ (see Table III).

IV. ANALYSIS OF THE ANGULAR CORRELATION DATA

The method and the formalism of the particle-particle angular correlations used in the analysis of the $^{92}\text{Mo}(^3\text{He}, d\bar{p})$ and the $^{96}\text{Zr}(^3\text{He}, d\bar{p})$ reactions are the same as those used in our previous studies of the proton decay of unbound IAS in the f - p shell nuclei.^{1,2} Therefore, only the main formulation and results of that method will be presented here.

TABLE II. Optical model potentials. The potentials for ^3He and d were of the form $V(r) = V_c - Vf(x_0) + (\hbar/m_p C^2)^2 V_{s0}(\sigma \cdot l) \frac{d}{dr} f(x_{s0}) - i[Wf(x'_0) - 4W_D d/dx'_0 f(x'_0)]$ where $f(x_i) = (1 + e^{x_i})^{-1}$, $x_i = (r - r_i A^{1/3})$, and $r_c = r_{oc} A^{1/3}$. V_c is the Coulomb potential, V , W , W_D , and V_{s0} are in MeV and the geometrical parameters in fm.

Particle	V	r_0	a_0	W	W_D	r'_0	a'_0	V_{s0}	r_{s0}	a_{s0}	r_{0c}
$^3\text{He}^a$	157.8	1.17	0.71	11.70	...	1.60	1.03				1.25
d^b	101	1.10	0.83	...	13.2	1.34	0.75	6.5	1.10	0.83	1.25

^a From Ref. 5.

^b From Ref. 20.

A. General

The angular correlation of the emitted proton, measured in coincidence in the (${}^3\text{He}, d\bar{p}$) reaction, using method II of Litherland and Ferguson²¹ can be written

$$N_i(\theta) = N_d(0^\circ) (\Omega_p/4\pi) [\bar{\Gamma}_p(i)/\Gamma] W(\theta), \quad (1)$$

with $N_i(\theta)$ the number of coincident protons emitted at an angle θ , $N_d(0^\circ)$ the number of single deuterons detected near 0° , Ω_p the solid angle of the proton detector, $\bar{\Gamma}_p(i)$ and Γ are, respectively, the proton partial width via channel i and the total width of the decaying state.

In geometry II of Litherland and Ferguson, the theoretical form of $W(\theta)$ expressed in the \mathcal{L} representation²¹ for the $A({}^3\text{He}, d\bar{p})B$ process is^{1,2}

$$W(\theta) = (2J_B + 1) 1/\Gamma \sum_{\substack{l_j l'_j \\ M_B, K}} (-1)^{2J_B - J_C - M_B - 1/2} \langle J_B J_B M_B - M_B | K 0 \rangle P(M_B) \\ \times (\pm \Gamma_{l_j}^{1/2}) (\pm \Gamma_{l'_j}^{1/2}) \times \cos(\gamma_{l_j} - \gamma_{l'_j}) \bar{Z}(l_j l'_j; \frac{1}{2} K) W(j J_B j' J_B; J_C K) Q_K P_K(\cos \theta). \quad (2)$$

The sum goes over K with $K_{\text{max}} \leq \min[2J_B, \max(2l), \max(2j)]$ and $|J_B - J_C| \leq j \leq |J_B + J_C|$. Here J_B and M_B are the spin and magnetic substates of the decaying state and J_C is the spin of the final state.

For the decay to the 0^+ ground state, only one proton partial wave l_j is present so that the nor-

malization coefficient of the angular correlation is equal to the ground-state branching ratio $\bar{\Gamma}_p(0^+)/\Gamma$. The deexcitation to final states with $J_C \neq 0$ involves competing partial waves l_j, l'_j with $l' = l + 2$ and $\sum_{l_j} \Gamma_{l_j} = \Gamma_p$.

For the case of the (${}^3\text{He}, d$) reaction on a spin 0 target, only $|M_B| = \frac{1}{2}$ and $\frac{3}{2}$ magnetic substates can be populated. $P(M_B)$ are defined as the population parameters and obey the normalization condition $\sum_{M_B} P(M_B) = 1$. The ratio

$$P_{3/2} = P(M_B = \frac{3}{2}) / [P(M_B = \frac{1}{2}) + P(M_B = \frac{3}{2})]$$

was treated as a free parameter to be determined in the analysis of the experimental data. The computer code GRILLE3 (Ref. 1) was used to determine the values of the population parameters, spins, and proton branching ratios which give the minimum χ^2 to the data using Eq. (2).

In addition, the population parameter $P(M_B)$ was calculated in the framework of the DWBA theory of direct reaction. The expression given in Ref. 1,

$$P(M_B) = \langle M_B | \rho | M_B \rangle = (2J_B + 1) |A_{l_s j}|^2 \sum_{m_a, m_b} |\beta_{s J_B}^{l m_a m_b}|^2, \quad (3)$$

where $A_{l_s j}$ and $\beta_{s J_B}^{l m_a m_b}$ are the usual spectroscopic coefficients and the reduced amplitudes²² were used to evaluate the ratio $P_{3/2}$ of the population parameters. The results were listed as intermediate outputs of the program VENUS with the optical parameters of Table II. For all the levels, the resulting values of $P_{3/2}$, at zero degree, were found to be very small ($< 1\%$). Therefore, the $M_B = \frac{3}{2}$ magnetic substate could only be populated through the finite solid angle of the 0° spectrometer.

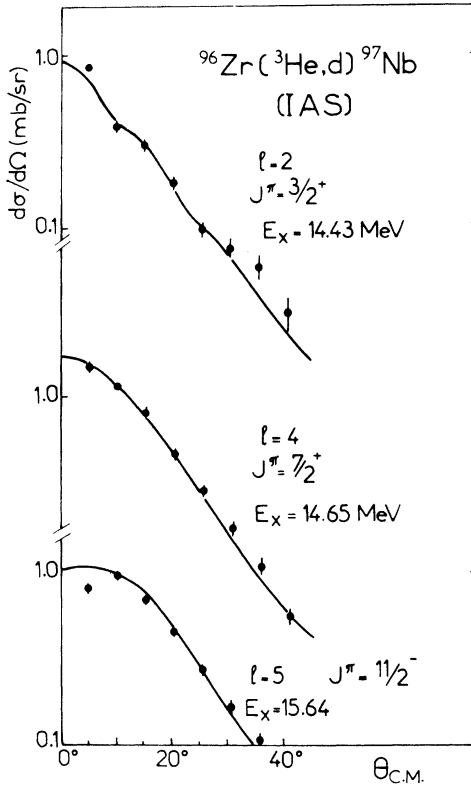


FIG. 8. Angular distributions of the ${}^{96}\text{Zr}({}^3\text{He}, d){}^{97}\text{Nb}$ reaction for the three IAS observed in this work. Vertical bars are statistical errors. Curves are DWBA predictions (for unbound states) for the indicated l values.

TABLE III. Summary of the results on IAS in ^{97}Nb from the $^{96}\text{Zr}(^3\text{He}, d)^{97}\text{Nb}$ reaction.

E_x (IAS) (MeV)	$E_p^{c.m.}$ ^a (MeV)	l	J^π	Γ_{sp}^{lJ} ^b (keV)	$S^\triangleright(^3\text{He}, d)$ ^b	$S^\triangleright(^3\text{He}, d)$ ^c	E_x (Parent) ^d (MeV)	S_{dp} ^d
14.43	6.97	2	$(\frac{3}{2})^+$	28.6	0.73	(1.0)	1.11	0.68
14.65	7.19	4	$(\frac{7}{2})^+$	1.66	0.98	1.15	1.26	0.60
15.64	8.18	5	$(\frac{11}{2})^-$	0.54	0.48	0.48	2.26	0.47

^a $E_p^{c.m.}$ is the energy of the resonance in the center-of-mass system. $E_p^{c.m.} = E_x(\text{IAS}) - B_p$. Here B_p is the binding energy of the proton in ^{97}Nb taken equal to 7.46 MeV.

^b Γ_{sp}^{lJ} is the single-particle width deduced from the Gamow state calculations. The spectroscopic factors $S^\triangleright(^3\text{He}, d)$ are defined by the expression $S^\triangleright(^3\text{He}, d) = (2T_0 + 1)C^2S$ where T_0 is the isospin of the target.

^c Reference 5.

^d Excitation energies and spectroscopic strengths for the parent states are from Ref. 18. The other values are from this work. The uncertainties on the excitation energies of the IAS in ^{97}Nb are of ± 30 keV.

B. Population parameters, spin assignments, and proton branching ratios

From this study of the $^{92}\text{Mo}(^3\text{He}, d\bar{p})$ and $^{96}\text{Zr}(^3\text{He}, d\bar{p})$ reactions, eight angular correlations are obtained for IAS in ^{93}Tc and ^{97}Nb decaying to the ground state and a number of angular distributions for levels decaying to the 2_1^+ , 3_1^+ , and other excited states of the target nuclei (^{92}Mo , ^{96}Zr). A comparison has been made between the experimental value $P_{3/2}^{\text{expt}}$ (which lead for a given spin assumption to χ^2 lower than the 0.1% confidence limit) and the predicted population of the $M_B = \frac{3}{2}$ magnetic substates $P_{3/2}^{\text{DW}}$ (for a given lJ transition and a cone of

detection of half angle ξ) in the framework of the DWBA theory of direct reactions due to finite solid angle effect. The quantities $P_{3/2}^{\text{expt}}$ and $P_{3/2}^{\text{DW}}$ are listed in Tables IV and V together with the adopted spin values and the measured proton branching ratios.

The J^π assignments listed in Tables IV and V for the IAS in ^{93}Tc and ^{97}Nb observed in this work were made using the following arguments:

- angular momentum transfer determined from the $(^3\text{He}, d)$ studies,
- spins determined from the independent model analysis of the $(^3\text{He}, d\bar{p})$ angular correlation data,

TABLE IV. Summary of the results of the $^{92}\text{Mo}(^3\text{He}, d\bar{p})^{92}\text{Mo}$ reaction.

E_x (MeV)	l^a	J^b	$P_{3/2}^{\text{expt}}$ ^c (%)	$P_{3/2}^{\text{DW}}$ ^c (%)	$\bar{\Gamma}_p(0^+)/\Gamma$ (%) g.s.	$\bar{\Gamma}_p(2^+)/\Gamma$ (%) 1.51 MeV	$\bar{\Gamma}_p(4^+)/\Gamma$ (%) 2.28 MeV	$\bar{\Gamma}_p(5^-)/\Gamma$ (%) 2.53 MeV	$\bar{\Gamma}_p(3^-)/\Gamma$ (%) 2.85 MeV	J^π ^d
8.41	2	$\frac{5}{2}^+$	1 ± 5	16	96 ± 6	< 3				$\frac{5}{2}^+$
9.78	4	$\frac{7}{2}^+$	20 ± 9	11	44 ± 6	41 ± 8	13 ± 3	< 3		$(\frac{7}{2})^+$
		$\frac{9}{2}^+$	37 ± 10							
9.90	2	$\frac{3}{2}$	1 ± 7	5	51 ± 7	37 ± 6	6 ± 2	< 3		$(\frac{3}{2})^+$
+	+	$\frac{5}{2}$	15 ± 7							
9.96	4	$\frac{7}{2}$	32 ± 7							$(\frac{7}{2})^+$
10.11	2	$\frac{5}{2}^+$	1 ± 7	5	44 ± 5	32 ± 4	9 ± 2	11 ± 3		$\frac{5}{2}^+$
10.74	5	$\frac{9}{2}^-$	23 ± 14							
		$\frac{11}{2}^-$	20 ± 12	15	19 ± 2	19 ± 2	14 ± 2	26 ± 3	23 ± 3	$(\frac{11}{2})^-$

^a l values are from the analysis of the $^{92}\text{Mo}(^3\text{He}, d)^{93}\text{Tc}$ reaction (Refs. 4 and 12).

^b Spin assumptions in agreement with the l determination and which give χ^2 values lower than the 0.1% confidence limit (see Fig. 9).

^c Experimental and calculated values for the population of the $M_B = \frac{3}{2}$ magnetic substate (see text, Secs. IV A and IV B). A cone of detection of half angle $\xi = 6^\circ$ has been taken to evaluate the population parameter $P_{3/2}^{\text{DW}}$.

^d Adopted spin values (see text, Sec. IV B).

TABLE V. Summary of the results of the $^{96}\text{Zr}(^3\text{He}, d\bar{p})^{96}\text{Zr}$ reaction.

E_x (MeV)	l^a	$J^\pi{}^b$	$P_{3/2}^{\text{exp}c}$ (%)	$P_{3/2}^{\text{DW}c}$ (%)	$\tilde{\Gamma}_p(0^+)/\Gamma$ (%)	$\tilde{\Gamma}_p(2^+)/\Gamma$ (%)	$\tilde{\Gamma}_p(3^+)/\Gamma$ (%)	$\tilde{\Gamma}_p(2^+)/\Gamma$ (%)	$\tilde{\Gamma}_p(5^+)/\Gamma$ (%)	$\tilde{\Gamma}_p(h)/\Gamma^a$ (%)	$\tilde{\Gamma}_p(h)/\Gamma^d$ (%)	$J^\pi{}^e$
14.43	2	$\frac{3}{2}^+$	18 ± 2	10	g.s.	1.76 MeV	1.90 MeV	2.33 MeV	3.07 MeV	(3.28 ± 0.05 MeV)	(4.20 ± 0.05 MeV)	$\frac{3}{2}^+$
14.65	4	$\frac{7}{2}^+$	15 ± 4	15	7 ± 3	10 ± 3	8 ± 2	7 ± 2				$(\frac{7}{2})^+$
			19 ± 5									
15.64	5	$\frac{5}{2}^-$	15 ± 11		3 ± 1.5	10 ± 3	5 ± 2					$(\frac{5}{2})^-$
			18 ± 10	22								

^a l values are from the study of the $^{96}\text{Zr}(^3\text{He}, d)^{97}\text{Nb}$ reaction.

^b Spin assumptions in agreement with the l determinations and which give χ^2 values lower than the 0.1% confidence limit.

^c Experimental and calculated values for the population of the $M_B = \frac{3}{2}$ magnetic substate (see text, Secs. IV A and IV B). A cone of detection of half-angle $\xi = 6^\circ$ has been taken to evaluate the population parameter $P_{3/2}^{\text{DW}}$.

^d Observed proton branching to highly excited states of ^{96}Zr . The centroid energies are also given (see discussion, Sec. IV B).

^e Adopted spin values (see text, Sec. IV B).

and

(c) comparison between the expected values of the population parameter $P_{3/2}^{\text{DW}}$ with the one obtained from the analysis of the angular correlation data.

The experimental angular distributions and the theoretical curves for protons decaying to the ground state of ^{92}Mo are shown in Fig. 9 together with typical examples of a least-square analysis (χ^2 plot versus population parameter $P_{3/2}$ for different assumptions). The same set of experimental data is presented in Fig. 10 for the $^{96}\text{Zr}(^3\text{He}, d\bar{p})^{96}\text{Zr}$ (g.s.) reaction. The angular correlation obtained for the ground-state analog in ^{91}Nb ($E_x = 9.86$ MeV, $J^\pi = \frac{5}{2}^+$) due to the isotropic abundance of ^{90}Zr in the ^{96}Zr is also reported. This state which is bound with respect to the neutron channel has a proton branching of (98 ± 3)% to the ground state of ^{90}Zr . This result together with a similar one obtained for the $2d_{5/2}$ ground-state analog in ^{93}Tc (see Table IV) is consistent with the one channel situation.

The experimental distributions of protons decaying to the various excited states of ^{92}Mo and ^{96}Zr nuclei were analyzed using Eq. (2). The population parameter $P_{3/2}^{\text{exp}}$ was held fixed to the value obtained in the analysis of the ground-state decay. Inelastic proton branching ratios $\tilde{\Gamma}_p(i)/\Gamma$ are listed in Tables IV and V. A detailed analysis of the inelastic decays for levels identified as IAS in ^{93}Tc and ^{97}Nb was carried out in order to obtain the amplitude of neutron coupling to target excited states in the parent level wave function and will be discussed in the next section.

The results of this analysis of the particle-particle angular correlations lead to the following conclusions:

(i) The analysis of the angular correlation data and the angular momentum transfer determined from the proton stripping studies can lead to a unique value for the spin J of the IAS ($2d_{5/2}$ and $2d_{3/2}$ IAS in ^{93}Tc and ^{97}Nb). However, unambiguous spin assignments have not been obtained for the $1h_{11/2}$ and $1g_{7/2}$ IAS in ^{93}Tc and ^{97}Nb because of the large error bars in the measured angular correlation data points (see Figs. 9 and 10).

(ii) Very accurate proton branching ratios are obtained for the decay to the ground and excited states of the ^{92}Mo nuclei. Due to the opening of the neutron channel, the corresponding values for the ^{96}Zr target are very low, but this method is able to detect proton branching as low as $3 \cdot 10^{-2}$ with 40% error bars. For the first time, experimental evidence is obtained concerning the rather large decay to the 2^+ , 3^- , and 5^- states. In particular the $1h_{11/2}$ IAS contains large components of the $2d$ and $3s$ waves coupled to the 5^- and 3^- first

excited levels of the targets. The most significant result is the evidence of highly excited configurations between 3.5 and 4.2 MeV in ^{96}Zr populated through the decay of the $1g_{7/2}$ and the $1h_{11/2}$ IAS in ^{97}Nb .

V. DISCUSSION AND INTERPRETATION OF THE RESULTS

The combined spectroscopic information from the distorted waves and angular correlation analysis is now presented. Seven states in ^{93}Tc and three states in ^{97}Nb are identified with the IAS of low-lying states of ^{93}Mo and ^{97}Zr on the basis of their excitation energies, spin and parity, and single-particle strength $S^>(^3\text{He}, d) = (2T_0 + 1)C^2S$ (here T_0 is the isospin of the target) as compared with S_{dp} number. The proton ground-state partial width Γ_p of the proposed IAS can be deduced from the $S^>(^3\text{He}, d)$ using the relation

$$S^>(^3\text{He}, d) = \Gamma_p / \Gamma_{sp}^{I,J}, \quad (4)$$

where $\Gamma_{sp}^{I,J}$ is the single-particle width evaluated

using the program GAMOW. Then the measured proton branching ratios can be used to obtain quantitative information on the inelastic proton partial widths through the measured $\bar{\Gamma}_p(i) / \bar{\Gamma}_p(0^+)$ ratios and the deduced $\Gamma_p^{I,J}$ elastic width from Eq. (4). In order to investigate the dependence of the $\Gamma_{sp}^{I,J}$ single-particle width on the method of calculation, the GAMOW $\Gamma_{sp}^{I,J}$ quantities for IAS in ^{93}Tc were compared with the ones calculated in the framework of the R matrix of nuclear reactions (Thompson, and Adams, and Robson²³). The results of this comparison are reported in Table VI together with the ones calculated by Bund¹⁵ in his analysis of the $^{92}\text{Mo}(^3\text{He}, d)^{93}\text{Tc}$ reaction to analog states. One could notice that the deduced single-particle widths are not dependent on the method used in the calculation within 20%. Although the single-particle widths can be considered as relatively well determined, the procedure mentioned above in order to extract absolute values for the inelastic partial waves $\bar{\Gamma}_p(i)$ is believed to be correct if the ground-state partial width $\bar{\Gamma}_p(0^+)$ determined in a $(^3\text{He}, dp)$ experiment can be identified with the "escape

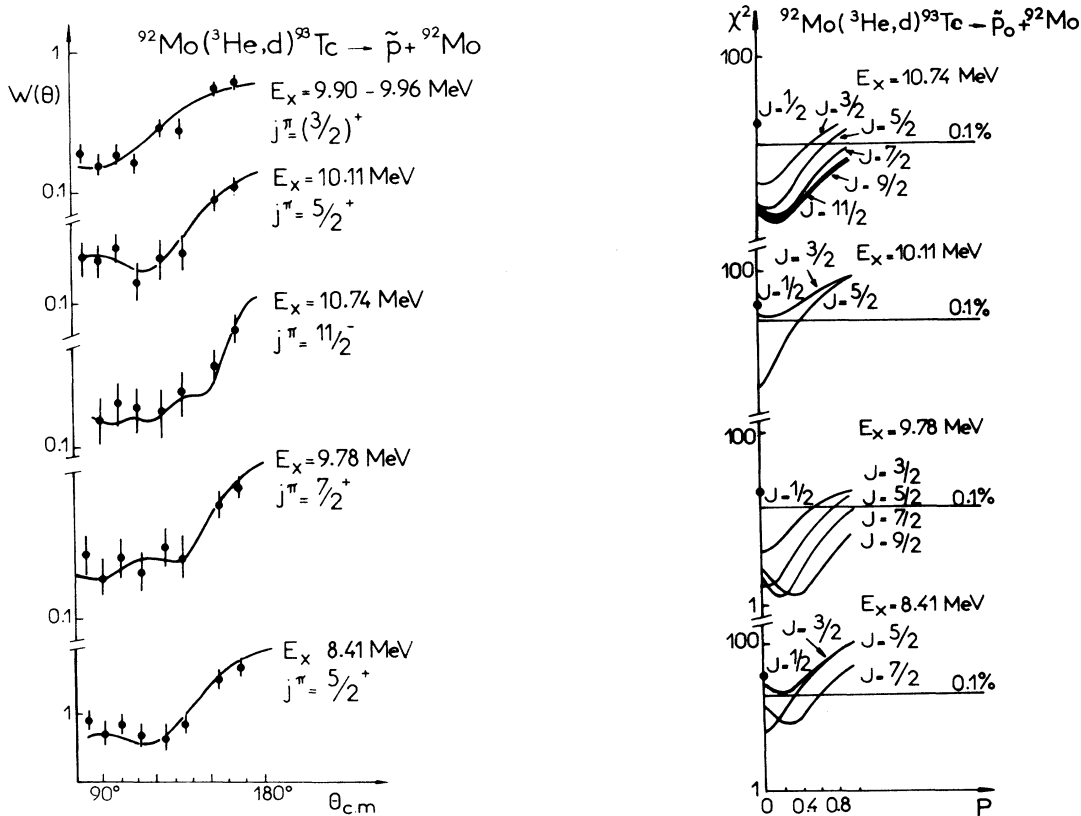


FIG. 9. (a) Angular correlation data for the $^{92}\text{Mo}(^3\text{He}, d)^{93}\text{Tc}$ (g. s.) reaction. Theoretical curves are calculated using Eq. (2) for the indicated J values. (b) On the right part of the figure are presented typical examples of the least-square analysis. χ^2 plots versus population parameter $P_{3/2}$ for different spin assumptions.

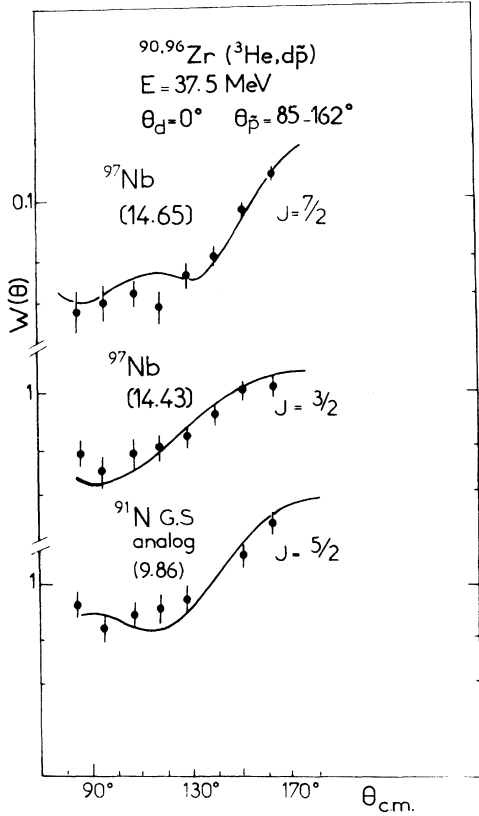


FIG. 10. Angular correlation data for the $^{90,96}\text{Zr}(^3\text{He}, d\bar{p})^{90,96}\text{Zr}(\text{g.s.})$. The theoretical curves are calculated using Eq. (2) for the indicated J values.

width" Γ_p . When the neutron channel is open for the particle decay of an IAS, the equality between $\bar{\Gamma}_p(0^+)$ and Γ_p has been verified [for example in the case of IAS in ^{49}Sc (Ref. 1)]. Therefore, one expects to be able to extract proper structure information on IAS in ^{97}Nb due to the very high ex-

TABLE VI. Comparison of single-particle widths of IAS in ^{93}Tc using different theoretical approaches.

$E_x(\text{IAS})$ (MeV)	l	J	$\Gamma_{sp}(G)^a$ (keV)	$\Gamma_{sp}(\text{TAR})^b$ (keV)	$\Gamma_{sp}(B)^c$ (keV)
8.41	2	$\frac{5}{2}$	1.55	1.50	1.46
9.78	4	$\frac{7}{2}$	0.24	0.26	0.25
10.11	2	$\frac{5}{2}$	20.0	15.0	21.0
10.74	5	$\frac{11}{2}$	0.19	0.15	0.12

^a Single-particle width calculated using the method of Coker *et al.* (Ref. 14).

^b The method of Thompson, Adams, and Robson (TAR) was used in this case (Ref. 23). The optical parameters of the proton optical potential are from Perey and Perey (Ref. 24).

^c Same quantities as defined in columns (a) and (b) from Bund (Ref. 15).

citation energies of these levels ($E_x \approx 15$ MeV, $B_n = 8.07$ MeV).

In the case of IAS in ^{93}Tc ($E_x = 8.5$ to 10.8 MeV, $B_n \approx 12.83$ MeV), the neutron channels are closed. The relation between these two quantities can be written²⁵

$$\bar{\Gamma}_p(0^+) = \Gamma_p + WP_0, \quad (5)$$

where W is the spreading width of the IAS and P_0 the probability for subsequent proton decay of "normal" $T_{<}$ states to the target ground state. Consequently, the extraction of core-excited components in ^{93}Mo low-lying parent levels will be affected by the rather large spreading width of the IAS in ^{93}Tc (Refs. 7–11) and the competition in the proton channel between background and analog states. Identification and decay properties of levels in ^{93}Tc and ^{97}Nb with the IAS of, respectively, ^{93}Mo and ^{97}Zr low-lying states are now discussed for each nucleus and each state according to its excitation energy.

A. Decay properties of IAS in ^{93}Tc

Some typical proton coincident spectra for the proposed IAS in ^{93}Tc are displayed in Fig. 11. Table VII summarizes the spectroscopic information deduced from this work. Examples of experimental angular correlations and theoretical predictions using Eq. (2) for IAS decaying to the first 2_1^+ , 4_1^+ , 3_1^- , and 5_1^- states of ^{92}Mo are shown in Fig. 12. Proton partial waves $2d_{5/2}$, $3s_{1/2}$, and $2d_{3/2}$ were used to describe the coupling of the $2d_{3/2}$ and $2d_{5/2}$ IAS to the 2^+ and 4^+ levels of the target. For the $g_{7/2}$ IAS, only $2d_{3/2}$, $2d_{5/2}$, and $1g_{7/2}$ waves were introduced in the analysis. Finally, for the $1h_{11/2}$ IAS, decay to the positive parity states (2_1^+ , 4_1^+) were analyzed using $1h_{11/2}$ proton waves, whereas the angular correlations obtained for the branching to the 5_1^- and 3_1^- states were analyzed using $2d_{5/2}$, $2d_{3/2}$, $1g_{7/2}$, and $3s_{1/2}$ partial waves.

The 8.41 MeV level. This level has been observed in two experiments in the proton elastic resonant channel.^{10,11} Graw *et al.*¹¹ using a polarized beam have established a spin and parity $J^\pi = \frac{5}{2}^+$ for this level. This level has also been observed in a number of proton stripping reactions.^{3,4,6,12} The deduced proton partial width from the elastic scattering experiments disagrees by a factor of 2 [0.75 keV (Ref. 10), 1.5 keV (Ref. 11)] as well as for the total width (respectively, 15 and 30 keV). From the measured spectroscopic strength $S^>(^3\text{He}, d)$, we can deduce, using Eq. (4), a proton partial width of 1.1–1.3 keV. The values of the spectroscopic factors $S^>(^3\text{He}, d)$ are in good agreement with the $S_{d,p}$ numbers of the parent states. A very weak branching ($\leq 3\%$) to the first excited 2^+

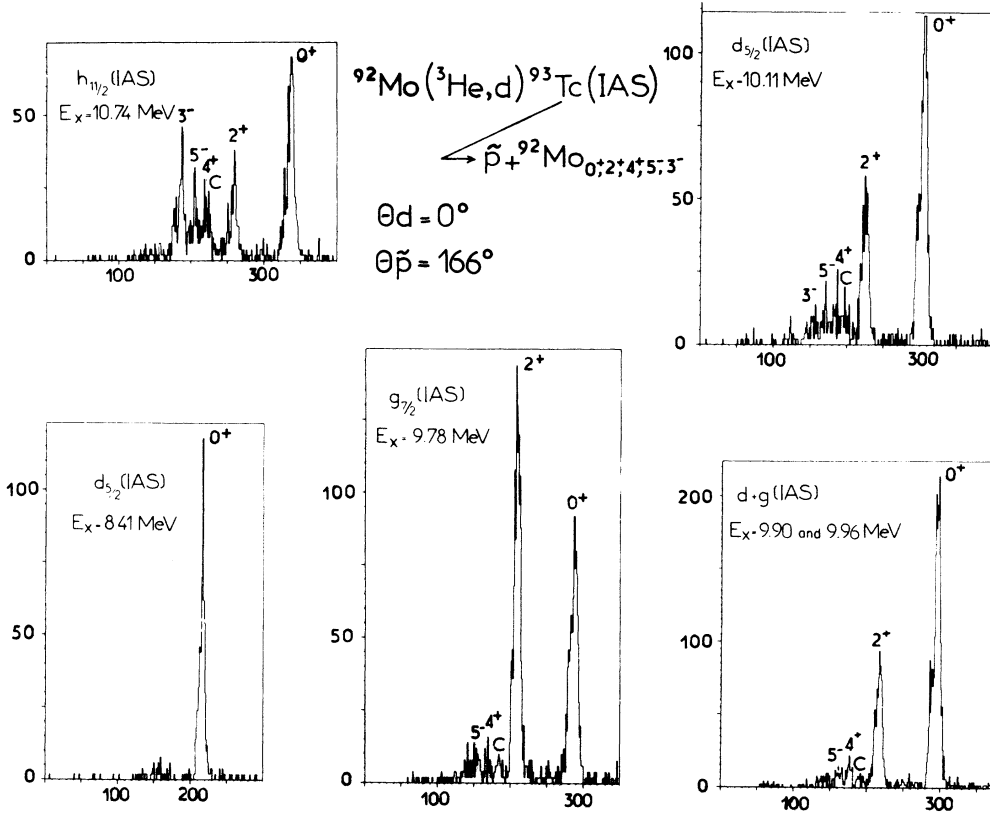


FIG. 11. Proton coincidence spectra showing the proton decay of IAS in ^{93}Tc . Notice the strong branching to the 5- and 3- states in the case of the $1h_{11/2}$ IAS.

state has been observed. The angular correlation analysis of the ground-state decay confirms the $J^\pi = \frac{5}{2}^+$ spin assignment from the polarization data.¹¹ Our results agree with the previous identification of this state as the ground-state analog in ^{93}Tc .

The 9.78 MeV level. In the $^{92}\text{Mo}(^3\text{He}, d)^{93}\text{Tc}$ reaction, this level is strongly populated. It has not been observed in the proton elastic and inelastic resonant channels and therefore, before this study, its decay properties have not been investigated. The angular correlation data to the ground state lead to a spin and parity $J^\pi = \frac{7}{2}^+, \frac{9}{2}^+$. The value $J^\pi = \frac{7}{2}^+$ has been adopted in agreement with previous proton stripping studies (see Table I). From the deduced spectroscopic factor and the single-particle width, listed in Table VI, we have deduced a ground-state proton partial width of 72 eV.

In order to extract inelastic proton partial widths, one can use the measured branching ratio $\Gamma_p(i)/\Gamma$ (see Table IV) and the deduced ground-state partial width Γ_p . The sum of the inelastic decays to the 2+ and 4+ states of the target obtained using this procedure should be considered as an upper limit due to the proton decay of the background T_c states [$\Gamma_p \neq \bar{\Gamma}_p(0^+)$] [see Eq. (5)] which cannot be separated from the decay of the IAS.

The analysis of the angular correlation to the 2+ and 4+ states involves dominant contributions from the $l = 0, 2$ ($3s_{1/2}, 2d_{3/2}, 2d_{5/2}$) proton partial waves. Although it is difficult to extract quantitative values for the various components ($2d_{5/2} \otimes 2^+$, $2d_{5/2} \otimes 4^+$, etc.) present in the wave functions of the parent levels, the observed large branching ratios to the excited states of the target clearly indicate strong core-excited components in the wave function of the $1g_{7/2}$ level in ^{93}Mo .

The 9.90–9.96 MeV levels. In the study of $^{92}\text{Mo}(p, p)^{92}\text{Mo}$ and $^{92}\text{Mo}(p, p')^{92}\text{Mo}$ reactions, an $l = 2$ resonance is observed around $E_p^{c.m.} = 5.80$ MeV.^{7,8,11} A close doublet has also been observed in proton stripping reactions at an excitation energy of 9.91, 9.94 MeV in ^{93}Tc .^{3,4,6,12} The angular distributions of this complex peak could only be reproduced by a mixture of $l = 2 + 4$ angular momentum transfer (see Table I) in agreement with the spectroscopic properties of the proposed parent states in ^{93}Mo ($E_x = 1.50$ MeV, $J^\pi = \frac{3}{2}^+$, $E_x = 1.53$ MeV, $J^\pi = \frac{7}{2}^+$). The spectrograph data of the present work, displayed in Fig. 1, clearly resolve this doublet of states. The $l = 4$ component of the doublet was not populated in the previous (p, p) or (p, p') resonant reactions studies.

TABLE VII. Summary of the spectroscopic properties of the IAS in ^{93}Tc .

E_x (IAS) (MeV)	$n_l J$	Γ^a (keV)	$\Gamma_p(0^+)$	$\sum \Gamma_p(2^+)^d$		$\sum \Gamma_p(4^+)^d$	$\sum \Gamma_p(5^-)^d$	$\sum \Gamma_p(3^-)^d$
			(keV)	(p, p) ^b	($^3\text{He}, d$) ^c	(p, p') ^b	($^3\text{He}, d\tilde{p}$)	($^3\text{He}, dp$)
8.41	$2d_{5/2}$	15	0.75					
								1.20
		30	1.50					
9.78	$1g_{7/2}$	n.o.	0.072		(0.067): $s_{1/2}$	(0.021): $s_{1/2}$		
					$d_{3/2}$	$d_{3/2}$		
					$d_{5/2}$	$d_{5/2}$		
9.90	$2d_{3/2}$	22	3.0					8.0
		27	5.0					
9.96	$1g_{7/2}$	n.o.	...	0.05				
10.11	$2d_{5/2}$	30	1.50					
		17		3.4	3.9	(2.5) : $s_{1/2}$	(0.7) : $d_{3/2}$	
						$d_{3/2}$	$d_{5/2}$	
						$d_{5/2}$	$g_{7/2}$	
10.74	$1h_{11/2}$	n.o.	...	0.085		(0.085): $h_{11/2}$	(0.062): $h_{11/2}$	0.115: $s_{1/2}$
								0.100: $d_{5/2}$
								$d_{3/2}$
								$g_{7/2}$
								$d_{5/2}$

^a The total widths Γ listed in this column are from Refs. 7, 8, 10, and 11. The notation n.o. indicates that these levels are not observed in proton resonant reactions.

^b The proton partial widths are from Refs. 7, 8, 10, and 11. The corresponding total widths are listed on the same line.

^c Proton elastic partial widths deduced from the relation $S^>(^3\text{He}, d) = \Gamma_p(0^+)/\Gamma_{sp}^{IJ}$ (see text Sec. V).

^d The sum of the inelastic partial widths $\sum \Gamma_p(i)$ to various final states are listed together with the proton waves used in the analysis of the corresponding angular correlations. The parenthesis indicates that these numbers are an upper limit (see text, Sec. V A).

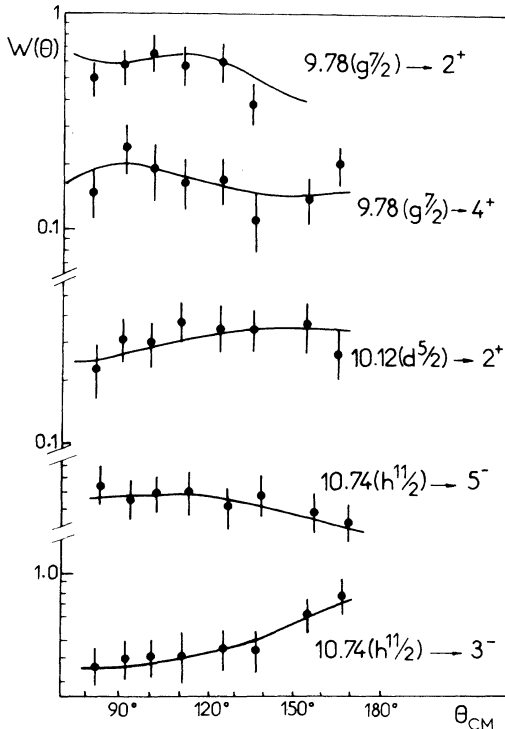


FIG. 12. Angular correlation data for the reaction $^{92}\text{Mo}(^4\text{He}, d)^{93}\text{Tc}(p_i)^{92}\text{Mo}(2^+, 4^+, 5^-, 3^-)$. Theoretical curves are for proton partial waves which are solutions of Eq. (2) and are listed in Table VII.

However, in the particle-particle angular correlation experiment this doublet has not been resolved and the proton branching ratios to the ground and excited states of the target contain the decay of both levels (see Table IV). Only the angular correlation to the ground state has a typical $J = \frac{3}{2}$ shape (see Fig. 9). The population of a $g_{7/2}$ analog state in the $^{92}\text{Mo}(^3\text{He}, d\tilde{p})$ data is clearly observed to contribute mainly to the decay of the first 2_1^+ and 4_1^+ levels of the ^{92}Mo nucleus.

The 10.11 MeV level. This level has been observed in various proton resonant reactions^{8,11} at an incident energy of $E_p = 6.01$ MeV. From both polarization measurements¹¹ and inelastic resonant decay study⁸ a spin and parity $J^\pi = \frac{5}{2}^+$ have been established in agreement with the properties of its parent state in ^{93}Mo (see Table I). The proton stripping reaction studies populate this state at $E_x = 10.11$ MeV in ^{93}Tc through an $l = 2$ angular momentum transfer. The angular correlation analysis has established a spin $J = \frac{5}{2}$ (see Table IV) for this level. From the deduced spectroscopic strength, the proton partial width to the ground state (3.4 keV, see Table VII) disagrees with the one measured in proton elastic experiment. As for the inelastic decay, a strong branching to the 2_1^+ state is observed. The sum of the inelastic widths is large and contains $l = 0 + 2$ proton partial waves. A weaker branch to the 4_1^+ and 5_1^+ states is

also evidenced in this work.

The 10.74 MeV level. This level has only been observed in the $(^3\text{He}, d)$ stripping reactions^{3,4,12} and is strongly populated at high incident energy ($E \geq 25$ MeV) through an $l=5$ angular momentum transfer. The proposed parent state carries an appreciable amount (40%) of the $1h_{11/2}$ neutron strength in ^{93}Mo .

The proton coincident spectra, displayed in Fig. 11, clearly indicate strong collective (2_1^+ , 4_1^+ , 5_1^- , and 3_1^-) components in the wave function of the parent level. The deduced proton elastic width ($\Gamma_p \approx 85$ eV) is very small and could explain why this level is not observed in proton resonant scattering experiments. The decay scheme of this high-spin analog state is measured here for the first time. Although the ground-state angular correlation cannot establish unambiguously a spin $J = \frac{11}{2}$ because of the very weak $\Gamma_p(0^+)/\Gamma$ branching ratio, this assignment is supported by the transfer reaction data and the spectroscopic properties of its proposed parent state ($E_x = 2.30$ MeV, $J^\pi = \frac{11}{2}^-$).

The measured angular distributions to negative parity levels could be fitted if one includes in the analysis the following collective components in the wave function: $[(s_{1/2} \otimes 5_1^-) + (d_{5/2} \otimes 5^-)]$ and $[(d_{3/2} \otimes 3_1^-) + (g_{7/2} \otimes 3_1^-)]$ (see Table VII).

B. Decay properties of IAS in ^{97}Nb

Typical proton coincident spectra for the $1g_{7/2}$ and $1h_{11/2}$ IAS in ^{97}Nb are presented in Fig. 13. The experimental angular correlations and theoretical predictions using Eq. (2) for the $2d_{3/2}$, $1g_{7/2}$, and $1h_{11/2}$ IAS decaying to the first 2_1^+ , 3_1^- or higher excited states of ^{96}Zr are shown in Fig. 14. Table VIII summarizes the spectroscopic information deduced from the combined analysis of the $^{96}\text{Zr}(^3\text{He}, d)^{97}\text{Nb}$ and the $^{96}\text{Zr}(^3\text{He}, d\bar{p})^{96}\text{Zr}$ reactions.

As mentioned before, the IAS in ^{97}Nb are unbound with respect to the neutron channel and therefore, proper structure information could be obtained, the surrounding T_ζ states decaying mainly through the neutron channel. The elastic proton partial widths have been deduced from Eq. (4) using the measured spectroscopic strengths $S^>(^3\text{He}, d)$ and the calculated single-particle widths $\Gamma_{sp}^>$.

From the measured ground-state branching ratio $\bar{\Gamma}_p(0^+)/\Gamma$ (see Table V), the total widths Γ of the IAS in ^{97}Nb have been deduced and are listed in Table VIII. Finally the sum of the inelastic widths $\sum \Gamma_p$, have also been determined using the $\bar{\Gamma}_p(0^+)/\Gamma$ and $\bar{\Gamma}_p(i)/\Gamma$ branching ratios (see Table V).

In addition to the observed decays to the first low-lying states (2_1^+ , 3_1^- , 2_2^+ , 5_1^- , etc.) of the target (^{96}Zr), the proton coincident spectra for the $1g_{7/2}$

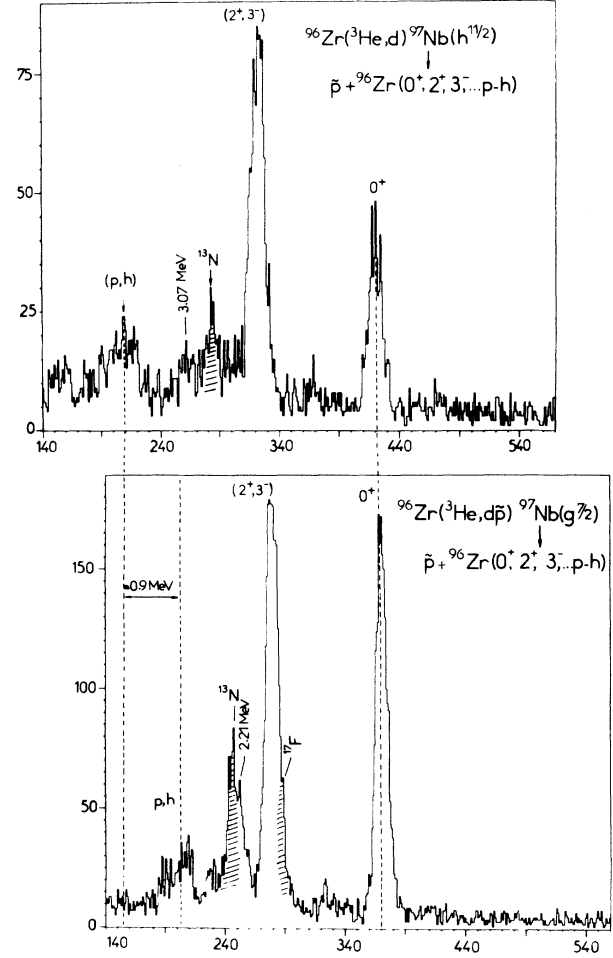


FIG. 13. Proton coincidence spectra showing the proton decay of the $1g_{7/2}$ and $1h_{11/2}$ IAS in ^{97}Nb . Note that the energy spacing between the two groups of highly excited states in ^{96}Zr (dashed lines) is approximately equal to the energy difference between the two IAS.

and $1h_{11/2}$ IAS in ^{97}Nb (see Fig. 13) present an enhanced population of levels at high excitation energy in ^{96}Zr . The centroid energy of these peaks is equal to 3.28 ± 0.05 MeV for the $1g_{7/2}$ IAS decay and to 4.20 ± 0.04 MeV in the case of the $1h_{11/2}$ IAS.

Two observations can be made in order to understand the nature of such highly excited levels:

(i) The difference in the excitation energies of these two peaks ($\Delta E = 0.92 \pm 0.09$ MeV) is very close to the difference between the excitation energies of the $1g_{7/2}$ and $1h_{11/2}$ IAS in ^{97}Nb ($\Delta E = 0.99 \pm 0.05$ MeV).

(ii) The $1g_{7/2}$ and $1h_{11/2}$ levels in the parent nucleus (^{97}Zr) contain large single neutron strengths (60 and 50%, respectively). The centroid energy of the neutron particle-hole multiplets in ^{96}Zr corresponding to the $(1g_{7/2})_p \otimes (2d_{5/2})_n$ and $(1h_{11/2})_p \otimes (2d_{5/2})_n$ configurations can be estimated using

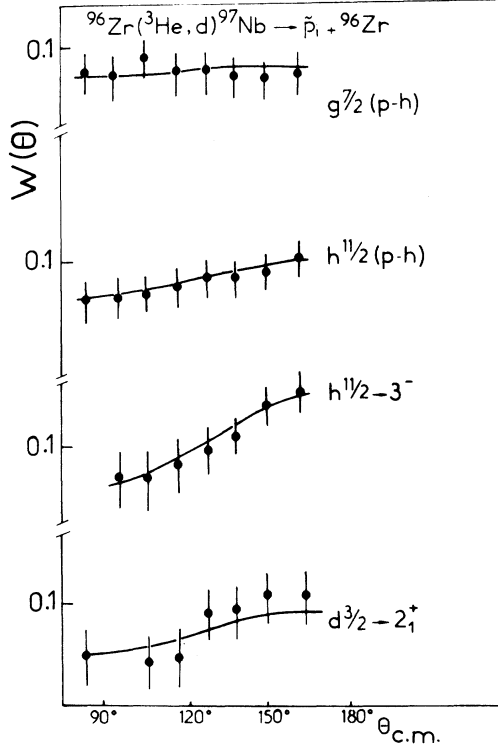


FIG. 14. Angular correlation data for the reaction ${}^{96}\text{Zr}({}^3\text{He}, d){}^{97}\text{Nb}(\bar{p}_i){}^{96}\text{Zr}$ (2^+ , 3^- , $p-h$). The notation $p-h$ is relevant to the decay to the neutron particle-hole region in ${}^{96}\text{Zr}$ (see text, Sec. V B). Theoretical curves are for proton partial waves which are solutions of Eq. (2) and are listed in Table VIII.

the relationships

$$\begin{aligned} \tilde{E}(1g_{7/2}, 2d_{5/2}) = & B_n({}^{96}\text{Zr}) - B_n({}^{98}\text{Zr}) \\ & + E_x(1g_{7/2}, {}^{97}\text{Zr}) + V_{p-h}, \end{aligned} \quad (6)$$

$$\begin{aligned} \tilde{E}(1h_{11/2}, 2d_{5/2}) = & B_n({}^{96}\text{Zr}) - B_n({}^{98}\text{Zr}) \\ & + E_x(1h_{11/2}, {}^{97}\text{Zr}) + V'_{p-h}, \end{aligned} \quad (7)$$

where $B_n({}^{96}\text{Zr})$ and $B_n({}^{98}\text{Zr})$ are, respectively, the binding energies of a neutron in ${}^{96}\text{Zr}$ ($2d_{5/2}$ ground state in ${}^{95}\text{Zr}$) and in ${}^{98}\text{Zr}$ ($3s_{1/2}$ ground state in ${}^{97}\text{Zr}$); $E_x(n\bar{j}, {}^{97}\text{Zr})$ are the excitation energies of the $1g_{7/2}$ and $1h_{11/2}$ levels in ${}^{97}\text{Zr}$ (see Table III); V_{p-h} and V'_{p-h} are the two-body interaction matrix elements between the $1g_{7/2}$, $1h_{11/2}$ neutron particle and the $2d_{5/2}$ neutron hole. In a first approximation, one can neglect the V_{p-h} and V'_{p-h} terms since an estimate on this term in the case of the $1g_{9/2}-2d_{5/2}$ particle-hole multiplet in ${}^{96}\text{Nb}$ leads to a value of 0.4 MeV.²⁶

We found a value of $\tilde{E}(1g_{7/2}, 2d_{5/2}) = 3.52$ MeV to be compared to $\tilde{E} = 3.28 \pm 0.05$ MeV and of $\tilde{E}(1h_{11/2}, 2d_{5/2}) = 4.52$ MeV instead of the experimental one of 4.20 ± 0.04 MeV. These two considerations are therefore strong arguments in favor of

TABLE VIII. Decay properties of IAS in ${}^{97}\text{Nb}$.

E_x (MeV)	nIJ	Γ (keV)	$\Gamma_p(0^+)$ (keV)	$\sum \Gamma_p(2^+)^a$ (keV)	$\sum \Gamma_p(3^-)^a$ (keV)	$\sum \Gamma_p(p-h)^a$ (keV)	$\sum \Gamma_p(p-h)^a$ (keV)	$\sum Spp'(2d_{5/2})^c$ J_F
14.43	$2d_{3/2}$	77 ± 14	28 ± 5	14	± 3	$s_{1/2} \otimes 2^+ : 0.26 \pm 0.10$ $d_{3/2} \otimes 2^+ : \text{small}$
14.65	$1g_{7/2}$	22 ± 10	1.6 ± 0.30	2.3 ± 1.0	...	1.5 ± 0.7	...	$d_{3/2} \otimes 2^+ : 0.3 \pm 0.15$ $g_{7/2} \otimes 2^+ : \text{small}$
15.64	$1h_{11/2}$	18 ± 10	0.55 ± 0.15	...	1.9 ± 0.9	$d_{5/2} \otimes 3^- : 0.11 \pm 0.05$

^a $\sum \Gamma_p(I^P)$ denotes the sum of the inelastic proton widths to the target excited states with spin and parity I^P . The excitation energies of the final states in ${}^{96}\text{Zr}$ are also indicated. $\sum \Gamma_p(p-h)$ represents the sum of the inelastic widths of the $1g_{7/2}$ and $1h_{11/2}$ IAS in ${}^{97}\text{Nb}$ decaying to highly excited levels (particle-hole region) of ${}^{96}\text{Zr}$. The centroid energy of the final states is also listed.

^b Spectroscopic factors for the $(n\bar{j}/I^P)_J$ configuration in the wave function of the $2d_{3/2}$, $1g_{7/2}$, and $1h_{11/2}$ parent levels in ${}^{97}\text{Zr}$ $Spp'(I^P) = \Gamma_p(I^P)/\Gamma_{sp}^{IJ}$ where Γ_{sp}^{IJ} is the single-particle width obtained from the Gamow state calculations.

^c $\sum_{J_F} Spp'(2d_{5/2}) = \Gamma_p(p-h)/\Gamma_{sp}^{25/2} \times \sum_{J_F} \Gamma_p(2d_{5/2}, J_F) / \Gamma_{sp}^{25/2}$ where $\Gamma_{sp}^{25/2}$ is the single-particle width for a $2d_{5/2}$ proton wave, J is the spin of the IAS, and J_F the spin of the final states in ${}^{96}\text{Zr}$: $J_F = (j \otimes 2d_{5/2})$; $J_F = 1^+$ to 6^+ for the $1g_{7/2}$ IAS and 3^- to 8^- for the $1h_{11/2}$ IAS.

the population of the neutron particle-hole $(1g_{7/2})_p \otimes (2d_{5/2})_h$ and $(1h_{11/2})_p \otimes (2d_{5/2})_h$ multiplets through the decay of the $1g_{7/2}$ and $1h_{11/2}$ IAS. When the proton decay energy is large, such decays have already been observed near the $N=82$ and $N=126$ neutron close shells in proton resonant inelastic reactions on isobaric analog states.²⁷ Assuming that we have correctly identified these multiplets and that they are rather pure, one can extract from Eqs. (6) and (7) and from the experimental centroid energies $\bar{E}(1g_{7/2}, 2d_{5/2})$ and $\bar{E}(1h_{11/2}, 2d_{5/2})$ the following values for the two-body interaction average matrix elements V_{p-h} and V'_{p-h} :

$$V_{p-h}(1g_{7/2}, 2d_{5/2}) = -0.24 \pm 0.06 \text{ MeV}$$

$$V'_{p-h}(1h_{11/2}, 2d_{5/2}) = -0.32 \pm 0.05 \text{ MeV.}$$

The nuclear structure information extracted for the $2d_{3/2}$, $1g_{7/2}$, and $1h_{11/2}$ IAS in ^{97}Nb will now be discussed.

The 14.43 MeV level. Its excitation energy, spin, parity, and spectroscopic strengths agree very well with the identification of this level as the analog state of the $E_x = 1.11$ MeV, $J^\pi = \frac{3}{2}^+$ first excited level of ^{97}Zr (see Table III). A significant width is observed to the ground and first excited states of ^{96}Zr (see Table VIII). Very low branching ($\leq 5\%$) has also been observed to the $E_x = 2.33$ MeV, $J^\pi = 2_2^+$ and to the $E_x = 2.75$ MeV, $J^\pi = 4_1^+$ levels of the target. The analysis of the angular correlation to the ground state has established a $J = \frac{3}{2}$. The measured angular distribution to the 2_1^+ presented in Fig. 14 could be fitted by a number of combinations of partial $3s_{1/2}$ and $2d_{3/2}$ proton waves. Because of the large difference between the proton penetrabilities of $l=0$ and $l=2$ waves, the solution which gave the larger $l=0$ contribution has been adopted. By dividing the measured inelastic width $\sum \Gamma_p(2^+)$ by the corresponding $3s_{1/2}$ single-particle width $\Gamma_{sp}^{0,1/2}$ one obtains a rather large ($3s_{1/2} \otimes 2^+$) core-excited component in the wave function of the $E_x = 1.11$ MeV, $J^\pi = \frac{3}{2}^+$ parent state (see Table VIII).

The 14.85 MeV level. The combined spectroscopic information from the $^{96}\text{Zr}(^3\text{He}, d)^{97}\text{Nb}$ and the $^{96}\text{Zr}(^3\text{He}, dp)^{96}\text{Zr}$ reactions lead to the identification of this level as the analog state of the $E_x = 1.26$ MeV, $J^\pi = \frac{7}{2}^+$ second excited state of ^{97}Zr (see Table III). The proton decay to the ground state is very weak ($\leq 8\%$) and the deduced small proton partial width makes its observation difficult in proton elastic resonant scattering. The decay to the 2_1^+ state could be reproduced by various mixing between $l=2$ ($2d_{3/2}$) and $l=4$ ($1g_{7/2}$) partial widths. For the same reason, as mentioned above, a pure $l=2$ wave leads also to a large ($2d_{3/2} \otimes 2^+$) component in the wave function of the parent state. The sum of the spectroscopic factors to the ground

state ($S^\lambda = 0.98$) and to the 2^+ state ($S_{p,p'} = 0.30 \pm 0.15$) exceeds the sum rule by a large amount. This could be explained by the large experimental errors in the deduced branching ratios for both the \bar{p}_0 (40%) and the \bar{p}_1 (30%) decay channels.

The most important result is the observation of a significant branching to a group of states located around ~ 3.3 MeV in ^{96}Zr in a region where the $(1g_{7/2})_p \otimes (2d_{5/2})_h$ multiplet is expected. The sum of the inelastic widths for this channel labeled $\sum \Gamma_p(p-h)$ in Table VIII, is of the same order of magnitude as the elastic width. Although the energy resolution in the proton channel was not sufficient to deduce separate angular correlations for each member ($J^\pi = 1^+$ to 6^+) of the multiplet, the angular distribution for the whole group could be reproduced assuming a pure $2d_{5/2}$ neutron hole (see Fig. 14). In order to obtain an estimate of the fullness of this configuration in ^{96}Zr , the spectroscopic factors were evaluated using the relation

$$\sum S_{p,p'}(2d_{5/2}) = \frac{\sum \Gamma_p(p-h)}{\Gamma_{sp}^{25/2}} \sum_{J_F} \frac{2J+1}{2J_F+1}, \quad (8)$$

where $\Gamma_{sp}^{25/2}$ is the $2d_{5/2}$ single-particle width, J the spin of the IAS and J_F the spins of the various members of the multiplet. In a pure shell-model picture of the ^{96}Zr nuclei, the $2d_{5/2}$ orbital is full and $\sum S_{p,p'}(2d_{5/2})$ should be equal to 6. Our experimental value is much larger (see Table VIII) which can be easily explained by the fact that a small admixture of a $3s_{1/2}$ wave ($\leq 20\%$) will strongly reduce the observed discrepancy. Such an occupancy of the $3s_{1/2}$ orbital in ^{96}Zr ground state agrees with a recent study of the $^{96}\text{Zr}(^3\text{He}, \alpha p)^{94}\text{Y}$ reaction.²⁸

The 15.64 MeV level. The measured angular momentum transfer and the deduced spectroscopic strength for this level supports its identification as the analog state of the $E_x = 2.26$ MeV, $J^\pi = \frac{1}{2}^-$ level in ^{97}Zr . Only a mean value for its ground-state proton decay has been obtained due to its very low branching ($\leq 3\%$). A relatively strong branching to the first 3^- level of ^{96}Zr has been evidenced and an upper limit of 5% has been deduced for its decay to the $E_x = 3.07$ MeV, $J^\pi = 5^-$ level of ^{96}Zr (see Table V). The 3_1^- angular correlation has been analyzed using $2d_{3/2}$ and $1g_{7/2}$ proton waves. Due to a ratio of about 27 between $l=2$ and $l=4$ single-particle widths and the observed small effect on the fit to the data obtained for the various mixing $l=2/l=4$ ratios, the adopted solution was the one with a pure $l=2$ $2d_{5/2}$ proton wave (Table VIII). This leads to a significant ($2d_{5/2} \otimes 3_1^-$) core-excited component but other large contributions, such as ($2d_{3/2} \otimes 5_1^-$) or ($3s_{1/2} \otimes 5_1^-$) in the wave function of the $\frac{1}{2}^-$ level in ^{97}Zr are suggested

by the observed branching to the 5_1^- state.

A strong group of states around 4.2 MeV in ^{96}Zr is populated through the decay of the $1h_{11/2}$ IAS. This structure is clearly shifted by the energy difference between the $1g_{7/2}$ and the $1h_{11/2}$ IAS with respect to the one already mentioned in the case of the $1g_{7/2}$ IAS decay (see Fig. 14). Its excitation energy agrees very well with the estimate of the $(1h_{11/2})_p \otimes (2d_{5/2})_h$ neutron particle-hole multiplet. From the measured branching ratio a total inelastic width $\sum \Gamma_p(p-h)$ of 0.28 ± 0.10 keV has been deduced. Using Eq. (8), we found that $\sum S_{pp}(2d_{5/2})$ is equal to 10 ± 5 and again the mean value is larger than the sum-rule limit of 6. Such a result [as well as the one obtained for the $(1g_{7/2})_p \otimes (2d_{5/2})$ particle-hole multiplet] should be taken as a qualitative estimate of the purity and/or the fullness of these final state configurations in ^{96}Zr . Additional effects as mentioned above could be explained by a small occupancy of the $3s_{1/2}$ orbital in the ^{96}Zr ground state and have not been taken into account in this analysis.

VI. SUMMARY

We have presented in this paper a rather comprehensive study of the decay properties of high-spin IAS near the $N=50$ closed shell. These studies have provided a large amount of new spectroscopic information on the $1g_{7/2}$ and $1h_{11/2}$ IAS in ^{93}Tc and ^{97}Nb . In addition to the strong population of these unbound levels by means of the $(^3\text{He}, d)$ reaction, the Gamow state form factor is found to be successful in reproducing both the shape and the spectroscopic strengths of the IAS in this region of the periodic table.

We would like to point out that the study of the sequential $(^3\text{He}, d\bar{p})$ process in a suitable geometry is a powerful tool for nuclear structure studies of high-spin analog states in heavy nuclei whereas this information could hardly be obtained in more standard proton elastic and inelastic resonant scattering. The main limitations of such an experimental approach have been demonstrated by comparing

IAS in ^{93}Tc , which are bound with respect to the neutron channel, and the ones in ^{97}Nb , which are unbound for both the neutron, proton, and α channels. In the first case, the competition between the decay of the IAS and the "normal" T_ζ states does not allow the extraction of direct structure information although a complete decay scheme can be established. For the IAS in ^{97}Nb , the opening of the neutron channel permits the determination of quantitative values for the core-excited components in the wave functions of the parent levels. However, the very low branching ratios could set a limit on the observed decay in this case.

Neutron particle-hole states are observed for the first time in ^{96}Zr through the decay of the $1g_{7/2}$ and $1h_{11/2}$ IAS. The deduced centroid energies will be useful in the search for such multiplets in direct inelastic (p, p') or (α, α') high resolution experiments on ^{96}Zr . Another limitation is encountered in the study of such closely spaced multiplets in heavy nuclei due to the obtained energy resolution in the proton channel. Although it will be difficult to achieve competitive energy resolution with the standard inelastic scattering studies, the selectivity of the $(^3\text{He}, d\bar{p})$ process, performed with improved energy resolution in both channels (d and \bar{p}), will probably allow the observation of high-spin multiplets near the $N=82$ closed neutron shell through the decay of the $1i_{13/2}$ and $1h_{9/2}$ IAS which have not been observed until now in resonant scattering experiments.

ACKNOWLEDGMENTS

We would like to thank Dr. J. L. Foster, Jr. for his help in the early stage of this work. We acknowledge L. Stab for the fabrication of the PSD and Si(Li) detectors, J. C. Artiges, P. Cohen, and A. Richard for their assistance in the electronic setup, and the operating crew of the Orsay M. P. Tandem Van de Graaff for the efficient running of the accelerator.

¹S. Galès, S. Fortier, H. Laurent, J. M. Maison, and J. P. Schapira, Phys. Lett. **56B**, 449 (1975); Nucl. Phys. **A268**, 257 (1976); **A259**, 189 (1976); **A265**, 213 (1976); Phys. Rev. C **14**, 842 (1976).
²S. Fortier, J. M. Maison, S. Galès, H. Laurent, and J. P. Schapira, Nucl. Phys. **A288**, 82 (1977).
³R. L. McGrath, N. Cue, W. R. Hering, L. L. Lee, B. L. Liebler, and Z. Vager, Phys. Rev. Lett. **25**, 663 (1970).

⁴D. Ashery, S. Alper, A. Moalem, Y. Shamai, A. I. Yavin, G. Bruge, A. Chaumeaux, and M. Moinester, Phys. Rev. C **5**, 1729 (1972).
⁵G. Finkel, D. Ashery, A. I. Yavin, G. Bruge, and A. Chaumeaux, Nucl. Phys. **A217**, 197 (1973).
⁶R. L. Kozub and D. H. Youngblood, Phys. Rev. C **4**, 535 (1971).
⁷C. F. Moore, P. Richard, C. E. Watson, D. Robson, and J. D. Fox, Phys. Rev. **141**, 1166 (1966).

- ⁸K. P. Lieb, T. Hausmann, and J. J. Kent, Phys. Rev. 182, 1341 (1969).
- ⁹N. Cue, I. Plessner, Z. Vager, and G. F. Wheeler, Nucl. Phys. A229, 429 (1974).
- ¹⁰H. Brändle, V. Meyer, and M. Salzmann, Nucl. Phys. A256, 141 (1976).
- ¹¹G. G. Graw, in *Polarization Phenomena in Nuclear Reactions*, edited by H. H. Barschall and W. Haeblerli (University of Wisconsin Press, Madison, 1971), p. 179.
- ¹²Y. Shamai, D. Ashery, A. I. Yavin, G. Bruge, and A. Chaumeaux, Nucl. Phys. A197, 211 (1972).
- ¹³S. A. A. Zaidi and W. R. Coker, Phys. Rev. C 4, 236 (1971).
- ¹⁴W. R. Coker and G. W. Hoffmann, Phys. 263, 19 (1973).
- ¹⁵G. W. Bund, Nucl. Phys. A233, 217 (1974).
- ¹⁶D. Ashery, S. Alper, A. I. Yavin, J. P. Longuequeue, D. Kong-A-Siou, and A. Giorni, Nucl. Phys. A179, 681 (1972).
- ¹⁷B. L. Cohen and O. V. Chubinsky, Phys. Rev. 131, 2184 (1963).
- ¹⁸C. R. Bingham and G. T. Fabian, Phys. Rev. C 7, 410 (1973).
- ¹⁹H. Laurent, J. P. Schapira, S. Fortier, S. Galès, and J. M. Maison, Nucl. Instrum. Methods 117, 17 (1974).
- ²⁰C. M. Perey and F. G. Perey, Phys. Rev. 152, 923 (1966).
- ²¹A. E. Litherland and A. J. Ferguson, Can. J. Phys. 39, 788 (1961).
- ²²G. R. Satchler, Nucl. Phys. 55, 1 (1964).
- ²³W. J. Thompson, J. L. Adams, and D. Robson, Phys. Rev. 173, 975 (1968).
- ²⁴F. G. Perey, Phys. Rev. 131, 745 (1963).
- ²⁵P. Richard, in *Nuclear Isospin*, edited by J. P. Anderson, S. D. Bloom, J. Cerny, and W. W. True (Academic, New York, 1969), p. 535.
- ²⁶J. P. Schiffer and W. W. True, Rev. Mod. Phys. 42, 191 (1976).
- ²⁷N. Stein, in *Nuclear Isospin*, edited by J. P. Anderson, S. D. Bloom, J. Cerny, and W. W. True (Academic, New York, 1969), p. 481.
- ²⁸S. Galès, Y. El Hage, S. Fortier, H. Laurent, J. M. Maison, J. P. Schapira, and J. L. Foster, Jr., Phys. Rev. C 17, 1308 (1978).